RESEARCH

Advancing respirable coal mine dust source apportionment: a preliminary laboratory exploration of optical microscopy as a novel monitoring tool

Nestor Santa[1] · Emily Sarver[1]

Abstract

Exposure to respirable coal mine dust (RCMD) can cause chronic and debilitating lung diseases. Real-time monitoring capabilities are sought which can enable a better understanding of dust components and sources. In many underground mines, RCMD includes three primary components which can be loosely associated with three major dust sources: coal dust from the coal seam itself, silicates from the surrounding rock strata, and carbonates from the inert 'rock dust' products that are applied to mitigate explosion hazards. A monitor which can reliably partition RCMD between these three components could thus allow source apportionment. And tracking silicates, specifically, could be valuable since the most serious health risks are typically associated with this component-particularly if abundant in crystalline silica. Envisioning a monitoring concept based on field microscopy, and following up on prior research using polarized light, the aim of the current study was to build and test a model to classify respirable-sized particles as either coal, silicates, or carbonates. For model development, composite dust samples were generated in the laboratory by successively depositing dust from high-purity materials onto a sticky transparent substrate, and imaging after each deposition event such that the identity of each particle was known *a priori*. Model testing followed a similar approach, except that real geologic materials were used as the source for each dust component. Results showed that the model had an overall accuracy of 86.5%, indicating that a field-microscopy based monitor could support RCMD source apportionment and silicates tracking in some coal mines.

1 Introduction

Exposure to respirable coal mine dust (RCDM) can cause lung diseases such as coal workers' pneumoconiosis, progressive massive fibrosis, and chronic obstructive pulmonary disease (Laney and Attfield 2010; Hall et al. 2019; Liu et al. 2021; Almberg et al. 2023). A recent systematic review conducted by Shekarian et al. (2023) found that the resurgence of CWP among coal workers can be attributed to various factors, such as geographic location, mine size, mining operation type, coal-seam thickness, coal rank, changes in mining practices, technology advancement, and engineering dust control practices. Ongoing or resurgent prevalence of occupational lung disease among coal miners in the US and elsewhere has underscored the importance of effective RCMD monitoring strategies (National and of Sciences, Engineering, and Medicine. 2018). Acknowledging the role of crystalline silica in many cases, a 2018 consensus report published by the National Academies of Sciences, Engineering, and Medicine called for development of real-time silica monitoring capabilities; it also called for an overall better understanding of dust sources, and development and/ or application of technologies to enable broad monitoring of RCMD trends (National and of Sciences, Engineering, and Medicine. 2018).

At present, real-time RCMD monitoring technologies only measure mass and particle concentrations, but not individual constituents. Indeed, there are only two types of

---

Nestor Santa and Emily Sarver have contributed equally to this work.

✉ Emily Sarver
   esarver@vt.edu

   Nestor Santa
   nsanta@vt.edu

[1] Department of Mining and Minerals Engineering, Virginia Tech, Blacksburg, VA 24061, USA

devices currently certified as intrinsically safe for use in US coal mines: The continuous personal dust monitor (CPDM, such as the PDM3700; Thermo Fisher Scientific, Waltham, Massachusetts) is mandated for regulatory compliance monitoring (per 30 CFR part 74), and measures mass concentration of respirable dust using a tapered element oscillating microbalance (Patashnick and Rupprecht 1991; Colinet 2022). A device called the personal DataRAM (pDR-1000; Thermo Fisher Scientific, Waltham, Massachusetts) is also permissible-though it has been recently discontinued by the manufacturer-and measures particle concentration in the respirable range using a light scattering technique (Listak et al. 2007). Despite significant interest, real-time monitoring of specific RCMD constituents like crystalline silica has not yet come to fruition. Beyond the considerable costs of research and development, and the niche context of coal mining environments, there is also the challenge of analytical sensitivity. For example, silica might only represent a small percentage of the total RCMD mass, which itself is relatively small. However, a viable alternative to monitoring specific constituents of RCMD could be to track larger components, which are often correlated. Current methods for obtaining real-time data and detailed information about the components of dust particles are either lacking or insufficient. The need for monitoring capabilities that can quickly and comprehensively analyze various physical and chemical characteristics of RCMD, such as their size, shape, distribution, and chemical constituents, is crucial for the advancement of portable monitoring technologies (Gozzi et al. 2016).

In many coal mines, the primary components of dust can be loosely associated with three main sources: (1) coal is sourced from the target coal seam itself; (2) silicate minerals such as aluminosilicates and silica are frequently sourced from the rock strata surrounding the coal seam; and (3) carbonate minerals such as calcite are frequently sourced from inert 'rock dust' products that are applied to mitigate explosion risks (Agioutanti et al. 2020; Jaramillo et al. 2022; Sarver et al. 2021; Keles et al. 2022). While other constituents can be present in RCMD, such as metal sulfides or oxides, they typically do not account for a substantial portion of mass or particle count (Sarver et al. 2019, 2021). Thus, in many mines, a simple partitioning of the RCMD into coal, silicates, and carbonates components in real-time (or near real-time) could enable source apportionment. Further, in mines where correlations can be established and periodically validated (e.g., via conventional sampling and laboratory analysis), tracking the silicates component of RCMD could serve as a proxy for silica.

Source apportionment is a well-established tool for understanding the origins of airborne particles and interpreting changes in composition (Thunis et al. 2019; Xue et al. 2022; Mondal and Singh 2021; Luo et al. 2022; Liu et al. 2022; Tohidi et al. 2022; Adeyemi et al. 2021; Das

et al. 2020). Most applications in the mining context have been focused on understanding the contributions of diesel engines (Cantrell 1987; McDonald et al. 2003; Bugarski et al. 2020). With respect to RCMD, there have been several studies aimed at determining the sources of silica, specifically (Schatzel 2009; Keles et al. 2022), and establishing the relative source contributions of dust, more broadly (Jaramillo et al. 2022; Trechera et al. 2022). However, all of these efforts have relied on samples collected at discrete times and analyzed in the laboratory. A real-time capability for source apportionment could enable a better understanding of changes in RCMD with mining and geologic conditions or dust controls.

Envisioning a field microscopy based monitoring solution, prior research by the authors showed that respirable-sized dust particles could be classified as either coal or minerals using just a pair of images (Santa et al. 2021). To explain, after collecting dust particles onto a glass sampling substrate, static images were collected in both plane-polarized (PP) and cross-polarized (CP) light. The PP image was used to identify all particles in the image frame; and the CP image was used to identify mineral particles in the frame, since they typically illuminate based on their birefringence. Supposing samples can be collected and imaged on a semi-continuous basis, this approach could support a simple binary classification of RCMD (i.e., mineral versus coal). This could be valuable on its own in certain applications, like tracking the relative dust generation from mining in rock strata versus the target coal seam at the production face (Santa et al. 2021). Moreover, in an environment where silica content is understood to correlate well with the overall mineral component of RCMD, even a crude measurement of the mineral component might be valuable if made frequently.

Nevertheless, an obvious limitation of a binary mineral/coal classification scheme is that it does not distinguish between different mineral components, which might have different sources and/or relatively different associations with RCMD constituents of interest, such as silica. To support source apportionment, the total minerals fraction of the dust needs to be further partitioned. The earlier work by the authors hinted at the possibility of minerals subclassification, highlighting preliminary efforts to distinguish carbonates from silicates-which might be a better proxy than total minerals for tracking silica. However, particle size was identified as a constraining factor. It can impact classification accuracy, as smaller particles may prove more challenging to identify due to the limitations of microscope resolution and interference from other particles.

This preliminary laboratory-scale study aims to evaluate the technical feasibility of utilizing a field microscopy-based RCMD monitor for source apportionment in a limited number of samples and mine materials. The main objective is to develop and test a particle classification model using a

direct measurement method that can effectively distinguish respirable-sized particles as coal, silicates, or carbonates. The study particularly examines the impact of particle size limits, as measured by projected area diameter (PAD), on improving the accuracy of the model.

2 Materials and methods

2.1 Dust materials

Four materials were used to develop the classification model: MIN-U-SIL® 5 and MIN-U-SIL® 10 (US Silica, Katy, TX, USA), which are high-purity quartz powders, were used as the source of silica particles. High-purity kaolinite powder (Ward's Science, Rochester, NY, USA) was used as a representative silicate source. Clean bituminous coal and a real rock dust product (obtained from an industry partner) were used as representative sources of coal and carbonates, respectively. While the silica, kaolinite and rock dust were obtained as powders, the coal required milling to enable respirable-sized particles to be sampled. It was pulverized and sieved to obtain -230 mesh material (< 63 μm) as the source of coal dust.

For model testing, the same coal and rock dust were again used as dust sources. However, to better represent the range of silicate minerals that might occur in RCMD (i.e., beyond pure silica and kaolinite) and determine if the optical characteristics of the silicates in real materials were comparable, three real rock strata materials were obtained from industry partners. The two materials designated as "ROM rock" represent the rock strata that was mined at the production face in two different operations (Mine 11 and Mine 14); these were hand-sorted from the run-of-mine (ROM) material on the production belt and were pulverized and sieved prior to sampling of respirable-sized particles. The material designated as "bolter dust" was obtained directly from the dust collection system on a roof bolter machine at Mine 16. This material was already fine and required no preparation prior to respirable sampling.

To validate the purity of the seven materials used in this work, respirable-sized particles of each material were analyzed by scanning electron microscopy with energy dispersive X-ray (SEM-EDX). Briefly, a sample of each material was collected in the lab using a 10-mm nylon cyclone at 2.0 L/min to discard over-sized particles. The dust was collected on 37-mm polycarbonate (PC) filters in closed styrene cassettes. A 9-mm subsection of each filter was cut and prepared for analysis by sputter coating with Au/Pd. Then, the computer-controlled SEM-EDX routine described by Sarver et al. (2021), Johann-Essex et al. (2017) was used to identify, size and collect elemental data on about 500 particles per sample in the 1–10 μm range. Per Sarver et al.

Table 1 Characterization of dust source materials by SEM-EDX

Material	Element (Mass %)			
	C	S	CB	Others[a]
Silica	1.07	98.93	0.00	0.00
Kaolinite	0.00	100.00	0.00	0.00
Rock dust	4.10	0.57	95.14	0.19
Coal	99.82	0.09	0.00	0.09
ROM rock (mine 14)	9.85	84.76	0.19	5.20
ROM rock (mine 11)	5.62	93.60	0.00	0.78
Bolter dust (mine 16)	9.20	89.40	0.20	1.20

C Carbonaceous; S Silicates; CB Carbonates

[a]Heavy minerals (e.g., Fe, Ti)

(2021), particles were classified using their elemental content, and the mass percentage in each class was estimated using particle dimensions and assumed values for specific gravity. The SEM-EDX work was conducted using an FEI Quanta 600 FEG environmental scanning electron microscope (ESEM) (Hillsboro, OR, USA). This microscope was equipped with a backscatter electron detector (BSD) and a Bruker Quantax 400 EDX spectroscope (Ewing, NJ, USA). The following parameters were used for SEM-EDX analysis routines: 1000x magnification, 12.5 working distance, 15 kV accelerating voltage, and a spot size of 5.5 μm. The resulting mass distribution of particles is shown in Table 1. The carbonaceous class is typically composed of coal particles; the silicates consist of silica, aluminosilicates, and other silicates; the carbonates are made up of calcium and magnesium carbonates; and the others class comprises heavy minerals such as Fe and Ti-rich minerals.

2.2 Respirable dust sampling and imaging

For both model development and testing, samples of respirable-sized dust particles were prepared in two stages: particles from a single source material were deposited on the sample substrate in the first stage, and then particles from a different material were deposited on the same substrate in the second stage. Samples were imaged after each stage, with images being captured on multiple areas ("frames") for each sample. The image frames were constant between stages, meaning that for a given sample the exact areas that were imaged after deposition of the first particle type were imaged again after deposition of the second particle type (Fig. 1). This process yielded a total of 34 samples (and 175 image frames) for model development, and another nine samples (153 frames) for model testing. The breakdown of samples and corresponding image frames is shown in Table 2. (For each two-material combination, the table also shows the number of particles sourced from each material type. These values were determined comparing the Stage 1
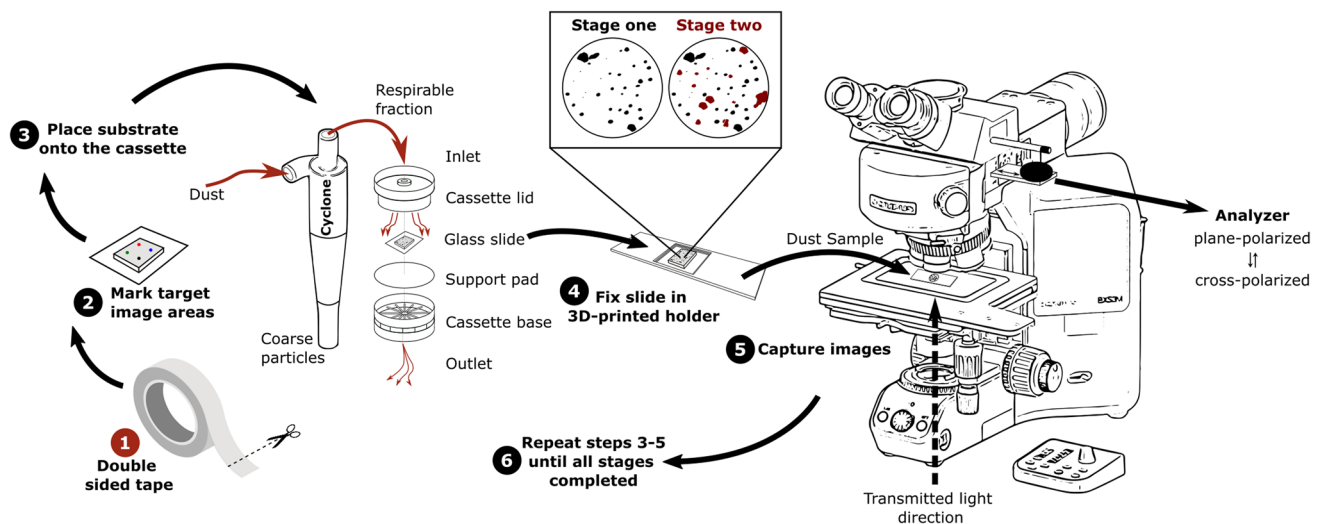
Fig. 1 Two-stage method used to prepare and image samples

Table 2 Dust image inventory

Material combination	Stage	Samples	Frames	Particles (per tracking)
Development				
Silica	1	19	93	667
Kaolinite	2			1769
Silica	1	10	45	319
Rock dust	2			508
Silica	1	5	37	101
Coal	2			1947
Total	–	34	175	5311
Testing				
ROM rock-mine 11	1	2	31	651
Rock dust	2			251
ROM rock-mine 11	1	1	16	131
Coal	2			1176
Bolter dust-mine 14	1	2	32	345
Rock dust	2			503
Bolter dust-mine 14	1	1	28	17
Coal	2			535
ROM rock-mine 16	1	2	31	920
Rock dust	2			434
ROM rock-mine 16	1	1	15	87
Coal	2			99
Total	–	9	153	5149

and Stage 2 images using a "particle tracking" approach as described below.)

The two-stage dust sampling and imaging procedure is illustrated in Fig. 1. This experimental design was specifically developed to allow direct classification of individual particles via particle tracking (described below). The sampling substrate was a small ($20\,mm \times 20\,mm$) piece of "sticky glass". It consisted of a glass coverslip (AmScope, Irvine, CA, USA) which was overlaid with double-sided clear acrylic tape (Maxwel Manufacturing, Hangzhou, China) to minimize dust particle loss during handling. Prior to the first stage of dust sampling, target imaging areas were marked on the tape surface using colored fine-tip markers such that the same areas could be visited after each sampling stage. For sampling, the sticky glass was mounted on top of a cellulose filter pad inside a closed 37 mm styrene cassette (Zefon International, Ocala, FL, USA). For each sampling event, the desired dust material was aerosolized in a small enclosure using pulses of compressed air. A small air pump was used to pull dust laden air from the enclosure, through a a 10-mm nylon cyclone and then through the cassette. At 2.0 L/min, the cyclone particle penetration approximates the ISO respirable convention (International Organization for Standardization 1995).

When considering a sampling airflow rate of 2.0 L/min, the efficiency curve of the 10-mm Dorr-Oliver nylon cyclone closely approximates the respirable dust criterion, as outlined by Tomb and Treaftis (1983), Page and Volkwein (2009). As per ISO standard 7708:1995, respirable dust refers to a fraction of inhaled airborne particles capable of penetrating beyond the terminal bronchioles into the gas-exchange region of the lungs. This fraction comprises particles smaller than 10 microns, with a mass median diameter of 4 microns. It should be noted that the sampling efficiency of the nylon cyclone may be influenced by factors such as orientation, wind speed, and sampling flow rate, as observed by Kar and Gautam (1995). Nonetheless, the particle size distribution obtained from analyzing the microscope
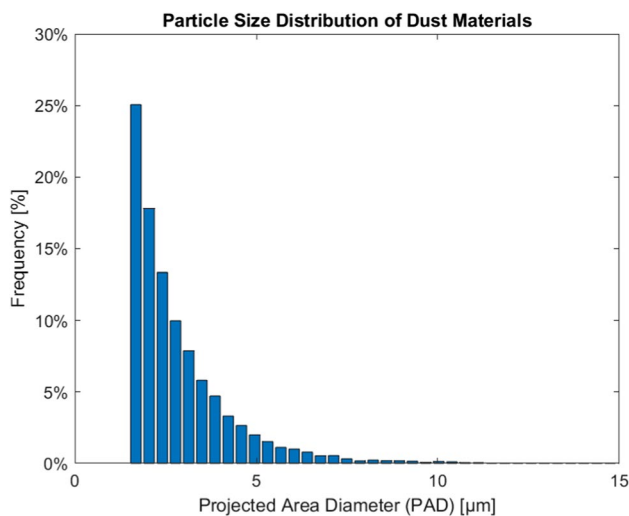
Particle Size Distribution of Dust Materials

Fig. 2 Particle size distribution for bulk materials used in Table 2

Table 3 Imaging acquisition settings

Settings	Value
Exposure time TPP	30.51 ms
Exposure time TCP	815.06 ms
LED light source intensity	50%
Red color adjustment	1.81
Green color adjustment	1.00
Blue color adjustment	1.28
Saturation	1.00
Gamma correction	1.00
Condenser aperture	0.40
Objective magnification	40x
Camera magnification	0.63x
Total calibrated magnification	25.008x
Image resolution	12-bit
Image file format	TIFF
Image height	2560 pixels
Image width	1920 pixels
Spatial calibration	87.971 nm/pixel

imagery from both the development and testing datasets indicates that the nylon cyclone can effectively separate the respirable fraction, as illustrated in Fig. 2.

After the first stage of sampling (i.e., deposition of the first particle type), the sticky glass substrate was carefully removed and mounted onto a house-made 3D-printed sample holder which was used to maintain an x-y reference point for the microscope stage. Then, under the microscope, the color-coded image frame marks were used to locate the target areas. For each area, an Olympus BX53M Polarizing Microscope and Stream Start 2.3 imaging software (Olympus,

Center Valley, PA, USA) were used to capture and save a pair of images: the first image was captured in transmitted plane-polarized light (TPP) and the second image was captured in transmitted cross-polarized light (TCP). Table 3 summarizes all the image acquisition settings, and a more detailed explanation of the settings was previously reported by Santa et al. (2021). After imaging, the substrate was carefully moved back to the sampling cassette and the second stage of particle deposition was completed with a different material. Finally, the same image frame areas were revisited to capture a new pair of images-again in TPP and TCP. In this way, the first pair of images only contained particles from the first material sampled, and the second pair of images contained particles from both materials.

2.3 Particle identification, feature extraction, and tracking

To identify individual particles in contrast to the background, the same particle identification approach detailed in Santa et al. (2021) was followed. Briefly, a local adaptive thresholding algorithm was used to classify image pixels into two categories: Foreground (particles) or background (substrate).[1] After performing morphological operations to clean edges and group particle pixels together, the output is a binary mask containing pixel category information. The binary mask was used to extract features for each individual particle including x and y location, size, circularity, and gray-scale intensity. In addition, the particle projected area diameter (PAD) was computed. Our analysis was limited to particles with a minimum PAD of 1.5 µm to reduce the influence of optical signals from particles beyond the resolution capabilities of the microscope. This measure was taken to minimize the impact of potential noise caused by small particles.

To assign a "true" identity (i.e., silica, kaolinite, coal, or rock dust) to each individual particle in each composite sample *a priori*, a particle tracking algorithm (see Algorithm 1) was developed and applied to each set of TPP images (i.e., captured on the same frame area of a following Stage 1, and then Stage 2 particle deposition). In essence, it works to determine whether a particle is present in both images (i.e., first particle type) or only in the Stage 2 image (i.e., second particle type), which enables direct classification based on its source material. Figure 3 illustrates the particle tracking approach using images for a particular frame area on a sample that

---

[1] Only the TPP images were used for identifying particles as they were found to be the most effective for this task in earlier work (Santa et al. 2021).
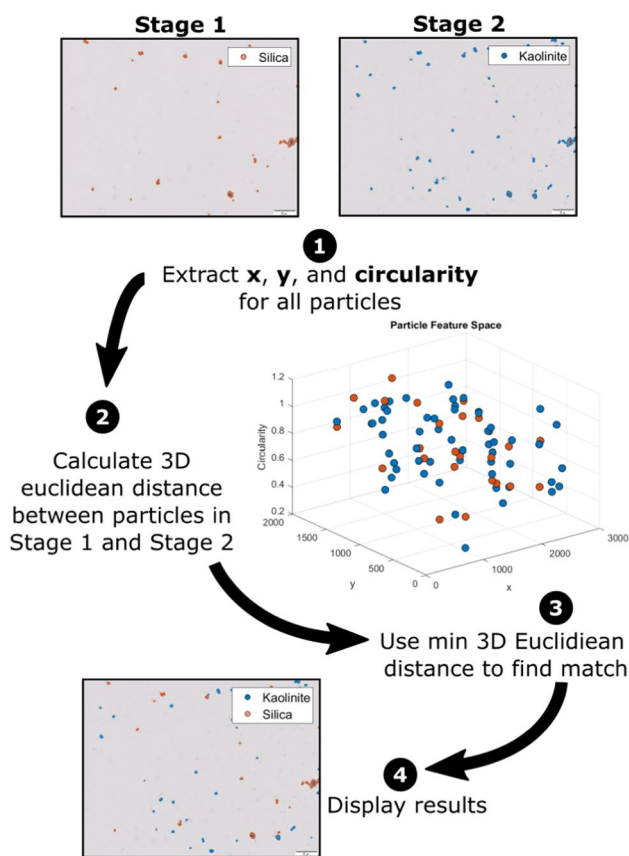
Fig. 3 Particle tracking approach

was first loaded with silica dust and then kaolinite dust. Using the binary masks described above, the tracking algorithm compares the *x* and *y* coordinates and circularity[2] for each particle identified in the Stage 2 image to each particle identified in the Stage 1 image. If a Stage 2 image and Stage 1 image particle match, the particle is assigned the Stage 1 particle type (e.g., silica in the example shown in Fig. 3); if a Stage 2 image particle does not have a match in the Stage 1 image, it is assigned the Stage 2 particle type (e.g., kaolinite in the example shown in Fig. 3). A match is defined as when the Euclidean distance (Eq. (1)) between particles in the feature space (i.e., for *x* and *y* coordinates, and circularity) is below some threshold. To determine the threshold for this task, a subset of the samples and image frames collected for model development were inspected to ensure the results matched the expected outcome closely. The

labels obtained by the particle tracking algorithm underwent a thorough comparative analysis against stage 1 and stage 2 images, whereby each particle's anticipated label was manually verified against its corresponding determined label in a subset of model development samples. The threshold value was chosen to maximize accuracy in particle label assignments. While the current work only included two stages of particle deposition and imaging, the same approach could theoretically be applied to samples generated using more stages.

$$\mathrm{d}(x, y, \mathrm{circ}) = \sqrt{(x_2 - x_1)^2 + (y_2 - y_1)^2 + (\mathrm{circ}_2 - \mathrm{circ}_1)^2}$$

(1)

Algorithm 1. Algorithm used to identify and track dust particles collected during sequential deposition

Algorithm 1 Particle Tracking Algorithm

1: initialize particle labels as stage 2
2: **for** each particle *p1* in image1 **do**
3:     $X1 \leftarrow$ create array $[x_1, y_1, circularity_1]$
4:     initialize *distance* as empty array
5:     **for** each particle *p2* in image2 **do**
6:         $X2 \leftarrow$ create array $[x_2, y_2, circularity_2]$
7:         $distance$.append(calculate_distance($X1, X2$))
8:     **end for**
9:     $m, ind \leftarrow$ find_minimum_distance($distance$)
10:     **if** $m \leq$ threshold **then**
11:         $p2(ind)$.label $\leftarrow p1$.label
12:     **end if**
13: **end for**

Figure 4 shows additional examples of particle tracking results for sets of Stage 1 and Stage 2 TPP images captured on three different samples (i.e., with silica + coal, silica + kaolinite, or silica + rock dust). These examples clearly illustrate how the particle tracking approach can be used for direct classification of individual particles that are loaded in stages from high-purity source materials. Thus, while the classification model being developed is intended to classify particles in real, composite samples (i.e., something akin to the Stage 2 images alone), the particle tracking results (i.e., as shown in Table 2) served as the "true" classification for each particle during model development. This allowed direct evaluation of model accuracy.
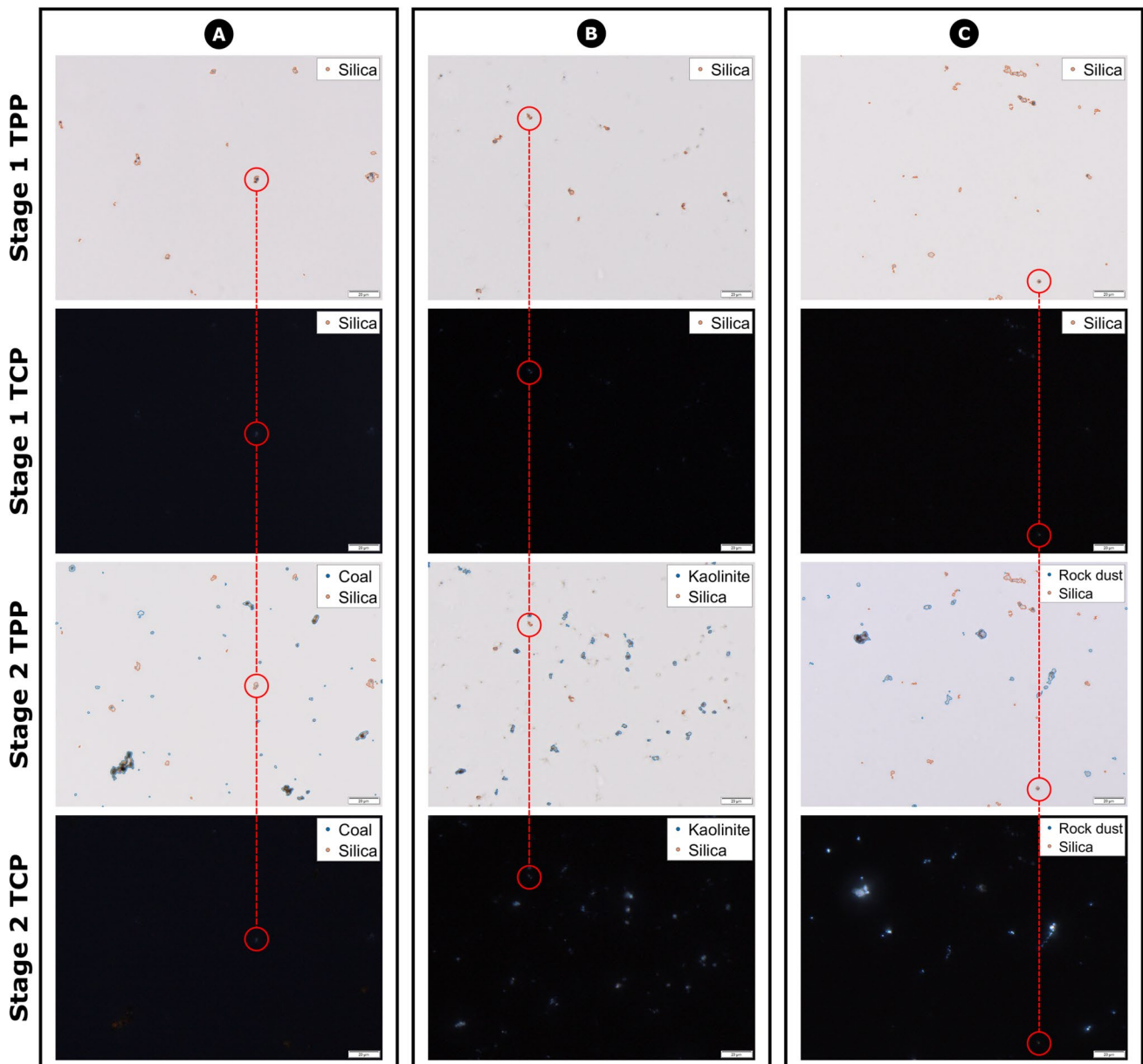
---

[2] *x*, *y*, and circularity were chosen as features for particle tracking working under the assumption that the particle location and shape should not dramatically change between sequential dust collection.

Fig. 4 Images of dust samples (**a**–**c**) initially loaded with silica during stage 1 under both TPP and TCP lighting conditions. Images in stage 2, show coal, kaolinite, and rock dust particles deposited on samples **a**–**c**, respectively. On TPP images, the particle boundaries have been determined for silica (orange), coal, kaolinite, and rock dust (blue) to show automated particle tracking between dust-loading events. Annotations (red) highlight dim silica particles on samples **a**–**c** during sequential dust deposition

3 Results and discussion

3.1 Model development

3.1.1 Particle classification

The images presented in Fig. 4 illustrate the distinctions in birefringence among various particle types. Notably, coal particles exhibit no birefringence, silica particles are characterized by minimal birefringence, kaolinite particles demonstrate moderate birefringence, while rock dust particles exhibit high birefringence. Such variations may be effectively utilized by a classification model in order to discern and categorize dust particles.

To build the particle classification model, all 175 pairs of TPP and TCP images that were captured following Stage 2 of dust particle deposition were used (i.e., see image frames for model development in Table 2). Based on the particle tracking algorithm, these included 1087 silica particles and 1769 kaolinite particles (2856 silicate particles in total),
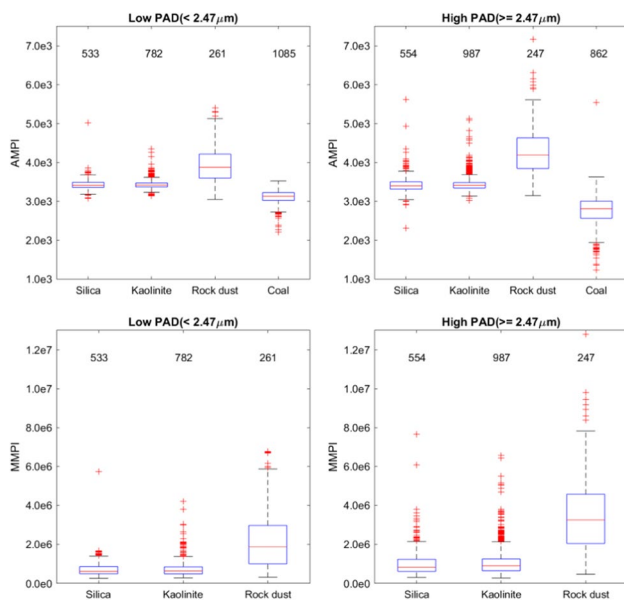
Fig. 5 Distribution of AMPI values observed for all particles in the model development data set. Data are split into two groups based on whether the PAD is above or below the median value observed for the entire data set (2.47 μm)

1947 coal particles, and 508 rock dust particles. As stated, the TPP binary mask was used to extract features for each particle, including the grayscale intensity. To establish classification thresholds, two grayscale intensity metrics were used: (1) The "added mean particle intensity" (AMPI) was calculated by summing the mean particle intensity observed in a TPP image with that in the paired TCP image. The AMPI exploits the birefringence of particles under TCP light to detect differences between minerals and coal. In RCMD, most minerals are expected to have anisotropic crystalline structures and thus be birefringent to some extent, whereas the coal is expected to be non-crystalline and thus non-birefringent (The AMPI metric was described in the earlier work by Santa et al. (2021)). (2) The "multiplication of the mean grayscale intensity" (MMPI) was calculated by multiplying the mean particle intensity observed in the TPP with that observed in the paired TCP image. The MMPI serves as a measure of the relative change in particle brightness between lighting conditions. It is expected that highly birefringent particles will have relatively higher MMPI values than less birefringent particles.

Figure 5 shows the distribution of AMPI and MMPI values, for all particles identified in the model development data set. For these figures, the results have been split into two categories to visualize the effect of particle size (as measured by PAD). The split between low and high PAD was made based on the median value observed across all particles in the model development data set ($n = 5311$). Consistent with expectations based on the earlier work (Santa

et al. 2021), higher PAD improved the separation between coal and mineral particles using the AMPI. Higher PAD also yielded improved separation between the mineral particle types (i.e., the two silicates versus rock dust) using MMPI. Given the relatively small number of particles with very high PAD included in the model development data set, additional splits in the data were not considered for the current work—though this should certainly be a focus of future efforts. Further, while reliable separation of silica and kaolinite using the MMPI does not appear feasible under the PAD conditions represented in Fig. 5, this could also be a topic for future research that seeks to classify silica, specifically. It is noted that, while particle loading density, i.e., number of particles within the image frame, did not appear to be an issue in the current work, this is a factor that likely would need to be controlled in a practical application. Simply put, if particles are in close proximity, they might interfere with one another (Santa et al. 2021).

Using the high PAD subset of the model development data shown in Fig. 5, AMPI and MMPI thresholds were set to separate the three primary components (i.e., coal, silicates and carbonates). From here, kaolinite and silica have been grouped together as 'silicates', and rock dust is now 'carbonates'. The AMPI and MMPI thresholds shown in Fig. 6 form the basis of a two-step classification model: in the first step, AMPI is used to classify a particle as either coal or mineral, and in the second step, MMPI is used to subclassify mineral particles as either silicate or carbonate. The threshold values were determined to minimize the differences between precision and recall across all three classes.

Precision is a statistical benchmark used to assess the accuracy of a model's positive predictions. To determine the precision, the number of true positive instances is divided by the total number of positive predictions made by the model Eq. (2). This proportion essentially quantifies the ability to predict positive instances correctly. (A high precision score indicates there are few false positives in the model predictions.) Recall, on the other hand, evaluates a model's ability to correctly identify all positive instances within a given dataset Eq. (3). Essentially, this measure gauges whether the model can capture all positive instances without missing any. Thus, recall is important for assessing false negatives (a high recall score indicates there are few false negatives.)

$$\text{precision} = \frac{\text{true positives}}{\text{true positives} + \text{false positives}} \tag{2}$$

$$\text{recall} = \frac{\text{true positives}}{\text{true positives} + \text{false negatives}} \tag{3}$$

In the domain of classification problems, the metrics of precision and recall are often found to be in tension with one another, with an increase in precision leading to a reduction

in recall, and vice versa. The choice of whether to optimize for precision or recall is dependent on the specific requirements of the problem. In this study, the two metrics were balanced to assess the overall performance of the model. To achieve this balance, the precision and recall values for each of the three classes (coal, silicates, carbonates) were evaluated, resulting in six values that were used to calculate the standard deviation. The standard deviation was used to determine the degree of difference between the values, with a high standard deviation indicating greater divergence and a low standard deviation indicating a more optimal balance.

A simple algorithm was employed to identify the combination of AMPI and MMPI thresholds that resulted in the minimum standard deviation (11.22%). The values of precision and recall that minimize the standard deviation are summarized in Fig. 6c. Based on the selected thresholds, an overall accuracy of 86.5% was observed for particles included in the model development image inventory Table 2 having PAD > 2.47 µm. As shown in Fig. 6, much of the misclassification was attributed to the overlap between the silicates and carbonates classes. In essence, some rock dust particles had relatively low MMPI values, while some silica and kaolinite particles had relatively high values.

3.2 Model testing

Next, the two-step classification model was challenged using the high PAD particles (PAD > 2.47 µm) included in the testing dataset shown in Table 2. As mentioned, the key difference between the dust particles in this data set and those used for model development was that the silicate particles were sourced from real mine materials (i.e., ROM rock and bolter dust, expected to contain a range of silicate minerals) rather than pure silica and kaolinite powders. It is noted that the real coal and rock dust particle sources were the same for both data sets, since these particle types are expected to be more similar across mines in terms of their optical features. I.e., Coal is generally expected to be non-birefringent, and carbonates are generally expected to be sourced from rock dust products which are often made from high purity calcite. The samples for model testing were generated and imaged using the same two-stage procedure used for the model development samples, and the images were processed using the same algorithms to find particles and extract feature data. Moreover, the particle tracking algorithm was applied to define the true source of each particle in the testing data set.
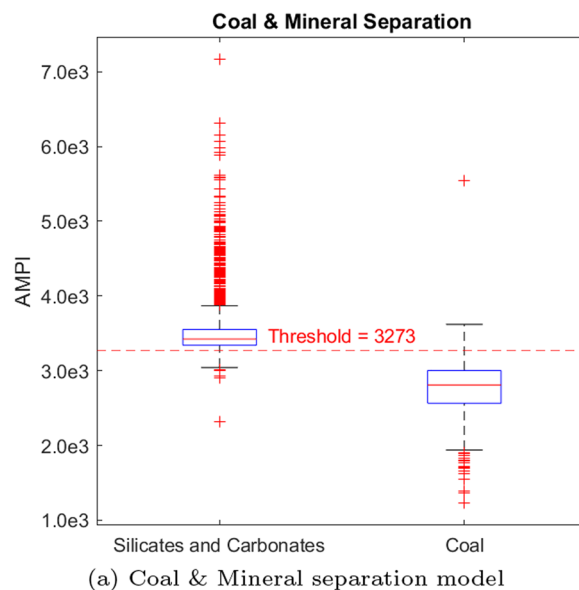
(a) Coal & Mineral separation model
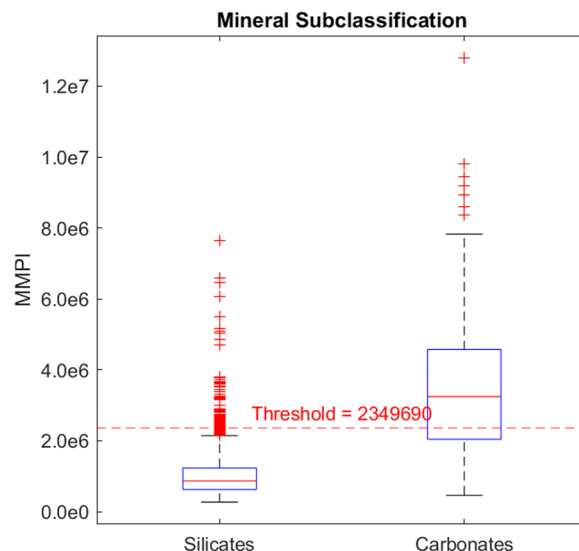
(b) Mineral subclassification model
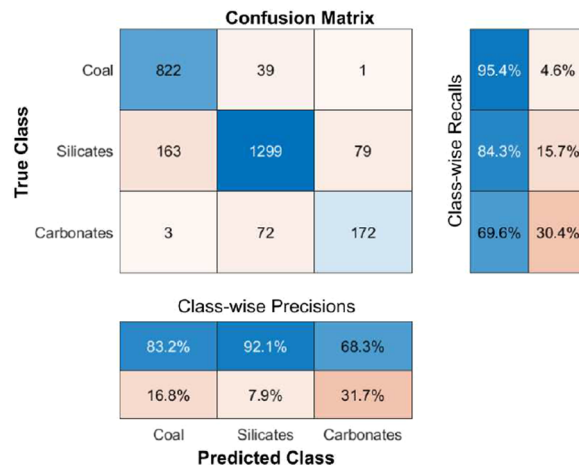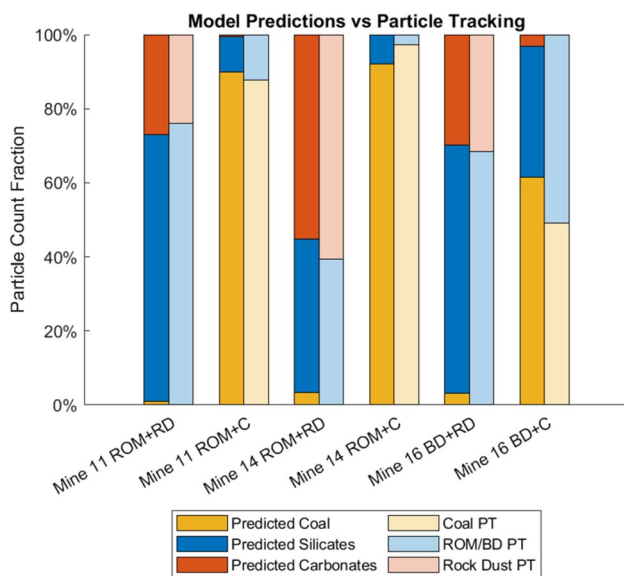

(c) Confusion Matrix

Fig. 7 Analysis on testing samples containing respirable dust deposited from three mine materials during stage one (mine 11 ROM rock, mine 14 ROM rock, and mine 16 bolter dust), followed by source dust deposition during stage two (rock dust or coal). Darker colors represent the results of the AMPI-MMPI classification model shown in Fig. 6. Lighter colors denote the results obtained by the particle tracking (PT) approach

Figure 7 compares the classification model results (i.e., based on particle AMPI and MMPI observed in the Stage 2 composite sample images) to the results of the particle tracking algorithm (i.e., particles classified based on their source material). On average the percentage difference across all results was 4%, and across all particle classes the average error was 4.54% for coal, 5.12% for silicates, and 2.34% for carbonates. The highest percentage difference between the predicted class and true source was 15.4% for estimating the silicates fraction in the sample containing Mine 16 bolter dust and coal (Mine 16 BD+C). Some discrepancies are probably due to misclassifications, which expected to happen more often between silicates and carbonates per Fig. 6. This is because there is some overlap between the range of MMPI values for silicate and carbonate particles. Additionally, silicate particles which have low birefringence may be incorrectly identified as coal particles (i.e., there is also some overlap in the range of AMPI values for silicate and coal particles).

Based on the higher average error noted above within the silicate class, it may be necessary to conduct calibration efforts on a mine-by-mine basis if this method were to be implemented in the field. This is important because if the silicates class holds for a broader range of minerals sourced from rock strata, such a classification scheme could help track the primary dust sources in coal mines (i.e., coal, rock dust, and rock strata).

Regarding the results shown in Fig. 7, another factor in observed discrepancies between the model classification and particle tracking results could be due to impurities present in the real ROM and BD source material. Impurities would not accounted for in the particle tracking approach to direct identification, because the tracking approach attempts to label a particle with its true source. This should work well for particles sourced from highly pure materials, but real source materials have some impurities. For example, per Table 1, respirable dust generated from the Mine 16 bolter dust material was dominated by silicates, but it had some carbonaceous particles. This might explain why the model predicts somewhat more coal than the particle tracking approach for samples containing this material. The consideration of the margin of error in real mine materials when utilizing the particle tracking approach is a crucial factor that can impact the accuracy of the model. Such errors can be carried over into the model-developing process and must be taken into account in any analysis of the data.

Nevertheless, the particle tracking approach developed for this work represents an important improvement upon the earlier work by the authors (Santa et al. 2021). Previously, images were not captured between sampling stages to identify particles in composite samples directly. Rather, SEM-EDX was employed for reference measurements. This was done by analyzing a paired sample for each composite sample that was imaged under the optical microscope, such that the overall class distribution determined by each method could be compared. Clearly, a more direct reference measurement (i.e., that does not require a separate analytical method on a separate sample) is superior for both efficiency and for minimizing uncertainties and errors.

Although source apportionment is the main objective of this study, the results presented here also imply that subclassification of silica particles might be possible in a particular PAD range. Specifically, particle classification may be improved as size increases. As noted above, when using a crude split between high and low PAD datasets, the results suggest that the classification of silica will be challenging. I.e., Even when considering particles with high PAD, there is a significant overlap between the silica and kaolinite MMPI values in Fig. 5. However, as PAD increases, differences in birefringence start to emerge. These results beg for further research in a somewhat larger PAD range.

While somewhat larger particles are not "respirable" by definition, some previous findings indicate that the distribution of particles in perhaps the 10–20 µm range might still be representative of the respirable distribution. For instance, analysis of airborne coal mine dust sampled with a respirable cyclone and with custom cyclones designed to cut at 10 or 20 µm showed that dust composition does not change much between those three fractions (Animah et al. 2023). Thus, the silica content in the 10–20 µm range may be a good proxy for

silica in the respirable range-especially if field microscopy based measurements can be initially calibrated to another method and validated periodically in a given environment.

4 Conclusions

The preliminary laboratory work presented here demonstrates that a simple optical microscopy approach could serve as the basis for field monitoring of RCMD. Particles in the respirable range can be separated into 3 main classes, which can support source apportionment in many mines. In addition, tracking the silica component in the larger fraction specifically could be a valuable proxy for silica in some mines.

If this method is to be used in coal mines, it may be necessary to conduct calibration and periodic validation work. This is crucial because proper classification of minerals can help identify the main sources of dust, including coal, rock dust, and rock strata.

The work here also implies the possibility for silica classification under favorable PAD conditions. The next step should focus on determining optimal particle size and loading density to subclassify silica particles.

The particle tracking approach utilized here is a useful technique for direct reference measurement, eliminating the need for SEM-EDX and increasing measurement efficiency while reducing uncertainty. Unlike SEM, the particle tracking method estimates dust constituents directly from image frames, allowing for high-confidence particle identification.

Finally, although samples have been prepared to contain the main dust constituents present in underground coal environments, and the materials used were all obtained from actual mine materials, further research should also include filter samples directly obtained from sampling campaigns in underground coal mines. This preliminary study is an important initial step towards comprehending the constituents and sources of RCMD. In order to achieve a comprehensive source apportionment analysis in the future, a wider range of dust materials from various mines will be required to better represent the complexity of RCMD in underground coal environments and assess the performance of the method described in this study.

Author contributions All authors contributed to the study conception and design. Material preparation, data collection and analysis were performed by NS. The first draft of the manuscript was written by NS and all authors commented on previous versions of the manuscript. All authors read and approved the final manuscript.

Data availability Not applicable

Declarations

Ethical approval and consent to participate Not applicable

Consent for publication Not applicable

Competing interests The authors have no competing interests to declare that are relevant to the content of this article.

References

Adeyemi A, Molnar P, Boman J, Wichmann J (2021) Source apportionment of fine atmospheric particles using positive matrix factorization in Pretoria, South Africa. Environ Monit Assess 193:1573–2959. https://doi.org/10.1007/s10661-021-09483-3

Agioutanti E, Keles C, Sarver E (2020) A thermogravimetric analysis application to determine coal, carbonate, and non-carbonate minerals mass fractions in respirable mine dust. J Occup Environ Hyg 17(2–3):47–58. https://doi.org/10.1080/15459624.2019.1695057

Almberg KS, Halldin CN, Friedman LS, Go LHT, Rose CS, Hall NB, Cohen RA (2023) Increased odds of mortality from non-malignant respiratory disease and lung cancer are highest among us coal miners born after 1939. Occup Environ Med 80(3):121–128. https://doi.org/10.1136/oemed-2022-108539

Animah F, Greth A, Keles C, Sarver E (2023) Effect of auxiliary scrubbers on respirable coal mine dust particle size and composition. In: Underground ventilation, pp 221–229

Bugarski AD, Hummer JA, Vanderslice S, Shahan MR (2020) Characterization of aerosols in an underground mine during a longwall move. Min Metall Explor 37(4):1065–1078. https://doi.org/10.1007/s42461-020-00209-6

Cantrell BK (1987) Source apportionment analysis applied to mine dust aerosols: coal dust and diesel emissions aerosol measurement. In: Proceedings of the 3rd mine ventilation symposium, pp 495–501

Colinet JF, Mischler SE (2022) Effectiveness of the cpdm in reducing overexposures to coal mine dust. Min Metall Explor 39:283–290. https://doi.org/10.1007/s42461-022-00563-7

Das A, Kumar R, Patel SS, Saha MC, Guha D (2020) Source apportionment of potentially toxic elements in street dust of a coal mining area in Chhattisgarh, India, using multivariate and lead isotopic ratio analysis. Environ Monit Assess 192:1573–2959. https://doi.org/10.1007/s10661-020-08321-2

Gozzi F, Della Ventura G, Marcelli A (2016) Mobile monitoring of particulate matter: state of art and perspectives. Atmos Pollut Res 7(2):228–234. https://doi.org/10.1016/j.apr.2015.09.007

Hall NB, Blackley DJ, Halldin CN, Laney AS (2019) Current review of pneumoconiosis among us coal miners. Curr Environ Health Rep 6:137–147. https://doi.org/10.1007/s40572-019-00237-5

International Organization for Standardization (ISO) (1995) Air quality: particle size fraction definitions for health-related sampling. Switzerland, Geneva

Jaramillo L, Agioutanti E, Ghaychi Afrouz S, Keles C, Sarver E (2022) Thermogravimetric analysis of respirable coal mine dust for simple source apportionment. J Occup Environ Hyg 19(9):568–579. https://doi.org/10.1080/15459624.2022.2100409

Johann-Essex V, Keles C, Sarver E (2017) A computer-controlled sem-edx routine for characterizing respirable coal mine dust. Minerals 7(1):15. https://doi.org/10.3390/min7010015

Kar K, Gautam M (1995) Orientation bias of the isolated 10-mm nylon cyclone at low stream velocity. Am Ind Hyg Assoc J 56(11):1090–1098. https://doi.org/10.1080/15428119591016304

Keles C, Pokhrel N, Sarver E (2022) A study of respirable silica in underground coal mines: Sources. Minerals 12(9):1115. https://doi.org/10.3390/min12091115

Laney AS, Attfield MD (2010) Coal workers' pneumoconiosis and progressive massive fibrosis are increasingly more prevalent among workers in small underground coal mines in the united states. Occup Environ Med 67(6):428–431. https://doi.org/10.1136/oem.2009.050757

Listak JM, Chekan GJ, Colinet JF, Rider JP (2007) Performance of a light scattering dust monitor at various air velocities: results of sampling in the active versus the passive mode. Int J Min Resources Eng 12(1):35–47

Liu S, Cheng W, Wang G, Fan L, Zhang R (2021) 4. Special issue on mine dust research: health effects and control technologies. Int J Coal Sci Technol 8(2):177–178. https://doi.org/10.1007/s40789-021-00434-4

Liu Y, Wang R, Zhao T, Zhang Y, Wang J, Wu H, Hu P (2022) Source apportionment and health risk due to pm10 and tsp at the surface workings of an underground coal mine in the arid desert region of northwestern china. Sci Total Environ 803:149901. https://doi.org/10.1016/j.scitotenv.2021.149901

Luo H, Wang Q, Guan Q, Ma Y, Ni F, Yang E, Zhang J (2022) Heavy metal pollution levels, source apportionment and risk assessment in dust storms in key cities in northwest china. J Hazard Mater 422:126878. https://doi.org/10.1016/j.jhazmat.2021.126878

McDonald JD, Zielinska B, Sagebiel JC, McDaniel MR, Mousset-Jones P (2003) Source apportionment of airborne fine particulate matter in an underground mine. J Air Waste Manag Assoc 53(4):386–395. https://doi.org/10.1080/10473289.2003.10466178

Mondal S, Singh G (2021) Pm2.5-bound trace elements in a critically polluted industrial coal belt of India: seasonal patterns, source identification, and human health risk assessment. Environ Sci Pollut Res 28(25):32634–32647. https://doi.org/10.1007/s11356-021-12876-z

National Academies, of Sciences, Engineering, and Medicine. (2018) Monitoring and Sampling Approaches to Assess Underground Coal Mine Dust Exposures. The National Academies Press, Washington, DC

Page SJ, Volkwein JC (2009) A revised conversion factor relating respirable dust concentrations measured by 10 mm dorr-oliver nylon cyclones operated at 1.7 and 2.0 l min-1. J Environ Monit 11:684–689. https://doi.org/10.1039/B817922K

Patashnick H, Rupprecht EG (1991) Continuous pm-10 measurements using the tapered element oscillating microbalance. J Air Waste Manag Assoc 41(8):1079–1083. https://doi.org/10.1080/10473289.1991.10466903

Santa N, Keles C, Saylor JR, Sarver E (2021) Demonstration of optical microscopy and image processing to classify respirable coal mine dust particles. Minerals 11(8):838. https://doi.org/10.3390/min11080838

Sarver E, Keles C, Afrouz SG (2021) Particle size and mineralogy distributions in respirable dust samples from 25 us underground coal mines. Int J Coal Geol 247:103851. https://doi.org/10.1016/j.coal.2021.103851

Sarver E, Keles C, Rezaee M (2019) Beyond conventional metrics: comprehensive characterization of respirable coal mine dust. Int J Coal Geol 207:84–95. https://doi.org/10.1016/j.coal.2019.03.015

Schatzel SJ (2009) Identifying sources of respirable quartz and silica dust in underground coal mines in southern west Virginia, western Virginia, and eastern kentucky. Int J Coal Geol 78(2):110–118. https://doi.org/10.1016/j.coal.2009.01.003

Shekarian Y, Rahimi E, Rezaee M, Roghanchi P (2023) 5. A systematic review of occupational exposure to respirable coal mine dust (RCMD) in the U.S. mining industry. Int J Coal Sci Technol 10(1):29. https://doi.org/10.1007/s40789-023-00586-5

Thunis P, Clappier A, Tarrason L, Cuvelier C, Monteiro A, Pisoni E, Wesseling J, Belis CA, Pirovano G, Janssen S, Guerreiro C, Peduzzi E (2019) Source apportionment to support air quality planning: strengths and weaknesses of existing approaches. Environ Int 130:104825. https://doi.org/10.1016/j.envint.2019.05.019

Tohidi R, Farahani VJ, Sioutas C (2022) Real-time measurements of mineral dust concentration in coarse particulate matter ($PM_{10-2.5}$) by employing a novel optical-based technique in los angeles. Sci Total Environ 838:156215. https://doi.org/10.1016/j.scitotenv.2022.156215

Tomb TF, Treaftis HN (1983) 6. Review of published de83 902993 experimental calibrations performed on the 10-millimeter nylon cyclone. Technical report, Mining Enforcement and Safety Administration

Trechera P, Querol X, Lah R, Johnson D, Wrana A, Williamson B, Moreno T (2022) Chemistry and particle size distribution of respirable coal dust in underground mines in central eastern Europe. Int J Coal Sci Technol 9(1):3. https://doi.org/10.1007/s40789-022-00468-2

Xue F, Niu H, Hu S, Wu C, Zhang C, Gao N, Ren X, Li S, Hu W, Wang J, Fan J (2022) Seasonal variations and source apportionment of carbonaceous aerosol in pm2.5 from a coal mining city in the north china plain. Energy Explor Exploit 40(2):834–851. https://doi.org/10.1177/01445987211043211